*J*ournal of *A*pplied *F*luid *M*echanics, Vol. 16, No. 1, pp. 131-145, 2023.
Available online at www.jafmonline.net, ISSN 1735-3572, EISSN 1735-3645.
https://doi.org/10.47176/jafm.16.01.1314

Ferrohydrodynamics Mixed Convection of a Ferrofluid in a Vertical Channel with Porous Blocks of Various Shapes

N. Guerroudj, B. Fersadou†, K. Mouaici and H. Kahalerras

Houari Boumediene University of Sciences and Technology, LTPMP, 16111, Algeria

†*Corresponding Author Email: bfersadou@usthb.dz*

(Received May 21, 2022; accepted September 11, 2022)

ABSTRACT

Numerical simulations of (water-Fe_3O_4) ferrohydrodynamics (FHD) mixed convection inside a vertical channel are performed. The magnetic field is produced by three sources positioned outside the channel's right wall. The latter is provided with localized heat sources surmounted by variously shaped porous blocks: rectangular, trapezoidal, and triangular. The general model of Darcy-Brinkman-Forchheimer is employed to describe the fluid flow in the porous regions, and the resulting equations are numerically solved by the finite volume approach. The influence of significant parameters, including the magnetic number (Mn), the Richardson number (Ri), and the shape of blocks, is examined. The results essentially reveal that the enhanced heat transfer brought by the magnetic field and its intensity increase is suppressed by the augmentation of Ri until a critical value, rising with Mn, beyond which the global Nusselt number increases again. The mean friction coefficient increases with increased Mn and reduced Ri. Compared to the case with no magnetic field, the maximum enhancement in heat transfer rate is around 132% for the rectangular blocks, 146% for the trapezoidal blocks, and 160% for the triangular blocks, while the maximum increase in pressure drop is approximately 45% for all the shapes. The triangular shape seems the most efficient because it leads to high heat transfer rates and low mean friction coefficients; its performance factor is 2.32 for a dominant magnetic field and 2.62 for a dominant buoyancy force. The current research's conclusions will help optimize the operation of various thermal engineering systems, including electronic devices, where the improved heat removal rate will keep the electronic components at a safe operating temperature.

Keywords: Ferrohydrodynamics; Mixed convection; Ferrofluid; Porous blocks; Blocks shape.

NOMENCLATURE

(a,b)	magnetic source coordinates
C	inertial coefficient
C_p	specific heat at constant pressure
d_f	molecule diameter of base fluid
d_p	nanoparticle diameter
Da	Darcy number
Ec	Eckert number
f	friction coefficient
g	gravitational acceleration
h	convective heat transfer coefficient
H	magnetic field
h_p	block height
I	electric current
k	thermal conductivity
k_B	Boltzmann's constant
K	permeability
ℓ	channel length
M	magnetization
Mn	magnetic number
Nu	Nusselt number
p	pressure
Pr	Prandtl number
T_{fr}	base fluid freezing temperature
(u,v)	components of velocity
W	channel width
w_p	block width at the base
w'_p	block width at the top
(x,y)	spatial coordinates

Greek symbols

β	thermal expansion coefficient
γ	shape angle
Υ_c, Υ_i	temperature ratios
ε	porosity
η_{fm}	mean friction coefficient ratio
η_{Nug}	global Nusselt number ratio
θ	dimensionless temperature
μ	dynamic viscosity
μ_o	magnetic permeability of the vacuum
ρ	density
φ	nanoparticles volume fraction

Subscripts

eff	effective

q	heat flux density	f	base fluid
Re	Reynolds number	g	global
Ri	Richardson number	i	inlet
R_k	thermal conductivity ratio	m	mean
R_μ	dynamic viscosity ratio	nf	nanofluid
R_η	performance factor	p	nanoparticles
s_p	spacing between two porous blocks	ref	reference
T	temperature	w	wall
T_c	Curie temperature		

1. INTRODUCTION

A promising method for enhancing heat transfer in many industrial thermal systems is to utilize ferrofluids. Indeed, under a variable magnetic field, the nanoparticles of this particular class of nanofluids are magnetized, the flow structure is altered, and the convective exchange is enhanced. Ferrofluids can be employed in various technology fields, including micro-scale heat exchangers, aerospace, biomedical, and electronic packaging. For this purpose, numerous experimental and numerical studies have been devoted to the problem of ferrofluid flow in the presence of a non-uniform magnetic field, also known as ferrohydrodynamics (FHD). Improvement of ferrofluid heat exchange by introducing one or more line dipoles was explored by Ganguly *et al.* (2004), Ghasemian *et al.* (2015), Larimi *et al.* (2016), Ghorbani *et al.* (2018), Nessab *et al.* (2019), Shah and Khandekar (2019), Mehrez and El Cafsi (2021), Shaker *et al.* (2021), and Dahmani *et al.* (2022). They found that vortices are formed locally in the dipoles' vicinity under the Kelvin force effect, which positively affects energy transport. The numerical investigation of Jarray *et al.* (2020) in a horizontal porous channel showed that by raising the Darcy number, the porosity parameter, and the Reynolds number, the FHD effect is significantly amplified. Ferrofluid viscosity and thermal conductivity dependence on magnetic field intensity and temperature were considered in the numerical work of Soltanipour (2021) in an annulus. To find a secure magnetic field that may be applied for therapeutic purposes, Teimouri *et al.* (2021; 2022) studied the impact of magnetic particles and external magnetic fields on the pulsatile blood flow in a stenosed curved artery in both rigid and elastic states. Vijai and Sharma (2022) examined a fluorocarbon-based magnetite nanofluid's FHD flow, heat, and mass transfer between two coaxial rotating stretchable disks. They used the semi-analytic homotopy analysis method and considered the viscosity dependence on depth and temperature. The motion of a nanomaterial within a cavity with a wavy heated wall was analyzed by Liu *et al.* (2022). They used two strategies to intensify the cooling process: inserting a wire close to the inner surface or adding a nano-sized substance to the water. By increasing the buoyancy force, the Nusselt number is enhanced by around 70.37% in the absence of a magnetic field. When FHD is applied, the heat transfer rate is improved by about 58.61%.

Several other researchers considered both MHD and FHD effects in different geometrical configurations and under various conditions: Sheikholeslami and Ganji (2014) inside a semi-annular enclosure, Gibanov *et al.* (2017) within a lid-driven cavity with a solid backward step at its bottom, Job and Gunakala (2018) in a corrugated channel with two heated porous blocks under an oscillating non-uniform magnetic field, and Aly and Ahmed (2020) in a square cavity containing an open circular pipe. Ghalambaz *et al.* (2020) analyzed nanofluids' heat and mass transfer in a hexagonal-shaped enclosure. The results revealed that the FHD and MHD effects have opposite impacts on transfer rates. 3D numerical simulations were performed by Mousavi *et al.* (2020) to study ferrofluid mixed convection inside a wavy channel. They showed that the combination of corrugation and magnetic field improved the heat transfer but increased the skin-friction factors. Natural convective heat transfer of a (Fe_3O_4/graphite slurry) non-Newtonian ferrofluid was explored numerically by Pishkar *et al.* (2022). The physical domain is a square enclosure provided with a heat source located at the bottom. The findings indicated that the rise in the magnetic number affects the heat transfer rate when the magnetic field source is close to the bottom wall's center.

Investigations on mixed convection in porous media were extensive because of its relevance in many practical applications, such as nuclear reactors, groundwater, drying processes, heat exchangers, solar collectors, geophysical systems, and electronic cooling. Many studies have been dedicated to this topic in various settings (Mejni and Ouarzazi 2009; Pal and Talukdar 2011; Alves *et al.* 2014; Chakkingal *et al.* 2020; Yerramalle *et al.* 2021). Bondarenko *et al.* (2019) and Çolak *et al.* (2021) showed that placing adherent or partially heated porous blocks in the center of a lid-driven cavity can significantly improve the heat transfer under specific conditions of blocks size, Darcy number, and heater position. The combination of constant magnetic fields, nanofluids, and porous media was considered in numerous papers, including that of Ali *et al.* (2020), where the authors also examined the effect of a rotating circular cylinder in a trapezoidal enclosure. Jakeer *et al.* (2021) investigated the influence of a heated obstruction's location within a lid-driven porous cavity. Recently, Alsedais *et al.* (2022) explored the roles of radiation and heat generation under the local thermal non-equilibrium condition in an undulating porous cavity containing a solid obstacle.

Fins, ribs, blocks, and other passive elements of various shapes have been employed to control heat transfer and pressure drop in thermal devices. The effect of rectangular, trapezoidal, and triangular porous/solid blocks and ribs was studied by Guerroudj and Kahalerras (2010; 2012), Seo *et al.* (2014), Behnampour *et al.* (2017), and Shamsi *et al.* (2017). The results indicated that the triangular shape performed best in most cases. Turbulent nanofluid flow in a channel was examined by Khetib *et al.* (2021) in the presence of a pin-fin heat sink. The considered pin fins shapes were hexagonal, circular, square, and triangular. The outcomes showed that circular fins and brick nanoparticles produced the best cooling performance and the lowest pressure drops.

According to this brief literature review, several studies considered the FHD effect on ferrofluid flow under various conditions. However, to the authors' knowledge, the works that additionally included a porous medium, such as those by Job and Gunakala (2018) and Jarray *et al*. (2020), are very limited. In this view, this paper provides a novel and attractive approach for improving heat transfer under mixed convection mode in a vertical channel by using simultaneously porous blocks of various shapes (rectangular, trapezoidal, and triangular), a non-uniform magnetic field, and a (Fe_3O_4-water) ferrofluid. Indeed, the porous medium creates an additional exchange surface and, in combination with the shape of the blocks, may cause less pressure drop. Adding Fe_3O_4 nanoparticles to the base fluid improves its thermophysical properties, and the application of an external non-uniform magnetic field alters the structure of the ferrofluid flow and delays the development of the thermal boundary layers, promoting thus the convective exchange. The effects of Kelvin and buoyancy forces intensity for various blocks shape are examined to obtain optimal conditions ensuring a high heat transfer gain for a low-pressure loss. Some practical applications of this study include designing and operating pressure sensors for biological fluids and cooling electronic devices such as RF switches in MRI apparatuses (Job and Gunakala 2018).

2. MATHEMATICAL FORMULATION

2.1 Physical Domain

The study domain, shown in Fig. 1, is a vertical channel consisting of two parallel plates of length ℓ separated by a distance W. The left plate is thermally insulated, while on the right one, porous blocks are mounted, each with a base width w_p, a height h_p, and spaced by a distance s_p. Localized heat sources, each providing a constant heat flux density q, are positioned under the blocks. The first block is placed in the channel so that inlet effects are avoided, while the length behind the last one is chosen large enough to satisfy the condition of a fully developed flow at the exit. Three blocks' shapes are considered, namely rectangular, trapezoidal and triangular. The passage from one shape to another is done either by varying the volume of a block (variable volume VV) or by keeping the volume constant (constant volume CV). In the VV case, the height h_p is kept constant, and the shape angle γ changes, whereas in the CV case, h_p and γ simultaneously vary (see Table 1). The relationship between the shape angle γ, the height h_p, the base width w_p, and the top width w'_p is the following:

$$\tan\gamma = 2\frac{h_p}{w_p - w'_p} \quad (1)$$

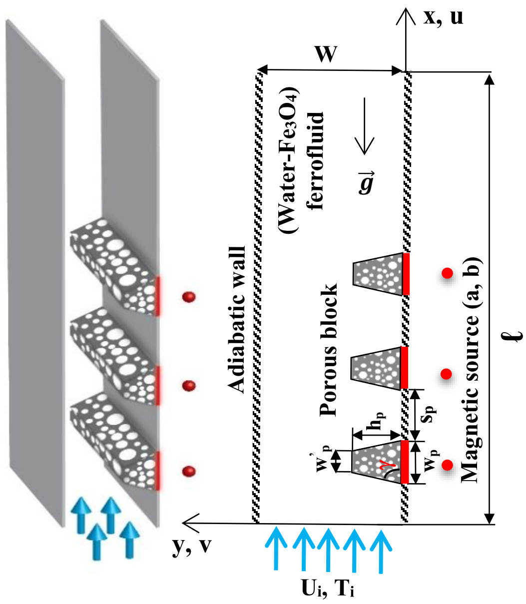

Fig. 1. Physical domain.

Table 1 Characteristics of the various block shapes

	Variable volume (VV)		Constant volume (CV)	
	h_p	γ (°)	h_p	γ (°)
Rectangular	0.6 W	90	0.3 W	90
Trapezoidal	0.6 W	63.4	0.4 W	55
Triangular	0.6 W	50.2	0.6 W	50.2

A (water-Fe_3O_4) ferrofluid, whose thermophysical characteristics are given in Table 2, penetrates the channel at a constant velocity, temperature, and nanoparticles volume fraction. A non-uniform magnetic field is created by three sources, each consisting of a wire traversed by an electric current I. The magnetic sources are placed outside the channel with their axial coordinate corresponding to the middle of each block, while the transverse distance b from the plate is 0.25W. The magnetic field's axial and transverse components are given by:

$$H_x(x,y) = -\frac{I}{2\pi}\frac{(y-b)}{(x-a)^2+(y-b)^2} \quad (2a)$$

$$H_y(x,y) = +\frac{I}{2\pi}\frac{(x-a)}{(x-a)^2+(y-b)^2} \quad (2b)$$

$$H(x,y) = \sqrt{H_x(x,y)^2 + H_y(x,y)^2} \quad (2c)$$

2.2 Governing Equations

The physical phenomenon of mixed convection in a vertical, partially porous channel is governed by a system of equations that require some assumptions to be solved.

Table 2 Thermophysical properties of water. and Fe_3O_4

Properties	Water	Fe_3O_4
C_p (J/kg K)	4179	670
ρ (kg/m³)	997.1	5200
k (W/m K)	0.613	6
β (1/K)	21×10^{-5}	1.3×10^{-5}

- The flow is two-dimensional, laminar, and in a steady state with the adoption of the Boussinesq approximation.

- The ferrofluid, considered incompressible and Newtonian, is treated as a homogeneous single-phase mixture.

- The nanoparticles, smaller in size than the porous matrix, are suspended in the base fluid with surfactants to avoid agglomeration and sedimentation problems.

- The porous medium is isotropic, homogeneous, and saturated by a single-phase fluid.

- Local thermal equilibrium between the base fluid, the nanoparticles, and the solid matrix.

- The viscous dissipation is not considered.

- The magnetic field induced by the fluid displacement is neglected compared to the applied external magnetic field.

Based on these assumptions and the Tiwari and Das model (2007) coupled with the general Darcy-Brinkman-Forchheimer model in the porous regions (Vafai and Tien 1981) to take into account the viscosity and inertia effects, the governing equations are written as follows (Tzirtzilaki 2005; Nield and Bejan 2013; Rosenweig 2013; Job and Gunakala 2018; Sheikholeslami and Shehzad 2018):

Continuity

$$\frac{\partial u}{\partial x}+\frac{\partial v}{\partial y}=0 \tag{3}$$

Momentum

$$\frac{\rho_{nf}}{\varepsilon^2}\vec{V}.\vec{\nabla}\vec{V}=-\vec{\nabla}p+\mu_{eff}\nabla^2\vec{V}-\frac{\mu_{nf}}{K}\vec{V}-\frac{\rho_{nf}C}{\sqrt{K}}|\vec{V}|\vec{V}+\rho_{nf}\vec{g}+\mu_0 M\vec{\nabla}H \tag{4a}$$

x direction

$$\frac{\rho_{nf}}{\varepsilon^2}\left(u\frac{\partial u}{\partial x}+v\frac{\partial u}{\partial y}\right)=-\frac{\partial p}{\partial x}+\mu_{eff}\left(\frac{\partial^2 u}{\partial x^2}+\frac{\partial^2 u}{\partial y^2}\right)-\frac{\mu_{nf}}{K}u-\frac{\rho_{nf}C}{\sqrt{K}}|\vec{V}|u+\rho_{nf}g\beta_{nf}(T-T_i)+\mu_0 M\frac{\partial H}{\partial x} \tag{4b}$$

y direction

$$\frac{\rho_{nf}}{\varepsilon^2}\left(u\frac{\partial v}{\partial x}+v\frac{\partial v}{\partial y}\right)=-\frac{\partial p}{\partial y}+\mu_{eff}\left(\frac{\partial^2 v}{\partial x^2}+\frac{\partial^2 v}{\partial y^2}\right)-\frac{\mu_{nf}}{K}v-\frac{\rho_{nf}C}{\sqrt{K}}|\vec{V}|v+\mu_0 M\frac{\partial H}{\partial y} \tag{4c}$$

Energy

$$(\rho C_p)_{nf}\vec{V}.\vec{\nabla}T=\vec{\nabla}(k_{eff}\vec{\nabla}T)-\mu_0 T\frac{\partial M}{\partial T}\vec{V}.\vec{\nabla}H \tag{5a}$$

$$(\rho C_p)_{nf}\left(u\frac{\partial T}{\partial x}+v\frac{\partial T}{\partial y}\right)=\left[\frac{\partial}{\partial x}\left(k_{eff}\frac{\partial T}{\partial x}\right)+\frac{\partial}{\partial y}\left(k_{eff}\frac{\partial T}{\partial y}\right)\right]-\mu_0 T\frac{\partial M}{\partial T}\left(u\frac{\partial H}{\partial x}+v\frac{\partial H}{\partial y}\right) \tag{5b}$$

$\mu_0 M\vec{\nabla}H$ stands for the Kelvin force, and $-\mu_0 T\frac{\partial M}{\partial T}\vec{V}.\vec{\nabla}H$ corresponds to the magnetocaloric effect. These two terms depend on the existence of the magnetic field gradient and the material magnetization, whose expression is (Tzirtzilakis 2005; Sheikholeslami and Ganji 2014; Sheikholeslami *et al.* 2015; Sheikholeslami and Shehzad 2018):

$$M=K'\,(T_c-T)\,H \tag{6}$$

In the non-porous region, the previous equations remain valid by taking: $\varepsilon = 1$, $K\to\infty$, $\mu_{eff}=\mu_{nf}$ and $k_{eff}=k_{nf}$.

2.3 Boundary Conditions

The associated boundary conditions are (Guerroudj and Kahalerras 2010; Guerroudj and Kahalerras 2012):

Inlet: $u=U_i, v=0, T=T_i$ (7)

Exit: $\frac{\partial u}{\partial x}=0, v=0, \frac{\partial T}{\partial x}=0$ (8)

Right wall: $u=v=0$

$$\begin{cases}\frac{\partial T}{\partial y}=-\frac{q}{k_{eff}} & \text{under the blocks}\\ \frac{\partial T}{\partial y}=0 & \text{elsewhere}\end{cases} \tag{9}$$

Left wall: $u=v=0, \frac{\partial T}{\partial y}=0$ (10)

2.4 Ferrofluid Properties

The ferrofluid properties are calculated using the following expressions:

Density

$$\rho_{nf}=(1-\varphi)\rho_f+\varphi\rho_p \tag{11}$$

Heat capacity

$$(\rho C_p)_{nf}=(1-\varphi)(\rho C_p)_f+\varphi(\rho C_p)_p \tag{12}$$

Viscosity and thermal conductivity

The Corcione mathematical model (Corcione 2011) is utilized to determine the ferrofluid's viscosity and thermal conductivity:

$$\mu_{nf} = \frac{\mu}{1-34.87\left(d_p/d_f\right)^{-0.3}\varphi^{1.03}} \tag{13}$$

$$\frac{k_{nf}}{k_f} = 1 + 4.4 Re_B^{0.4} Pr^{0.66}\left(\frac{T}{T_{fr}}\right)^{10}\left(\frac{k_P}{k_f}\right)^{0.03}\varphi^{0.66}$$
$$Re_B = \frac{\rho_f d_p}{\mu}\frac{2k_B T}{\pi\mu d_p^2} \tag{14}$$

$d_f = 3.85\times10^{-10}$ m and T_{fr} = 273.15 K are the base fluid's molecule diameter and freezing temperature, respectively.

2.5 Dimensionless Equations and Boundary Conditions

The system of equations and the boundary conditions are transformed into a dimensionless form using the following reduced variables:

$$(X,Y) = \frac{(x,y)}{W}, (U,V) = \frac{(u,v)}{U_i}, P = \frac{p}{\rho_{nf}U_i^2}$$
$$\theta = \frac{T-T_i}{qW/k_f}, \bar{H} = \frac{H}{H_0}, H_0 = \frac{I}{2\pi W}$$

$$\frac{\partial U}{\partial X} + \frac{\partial V}{\partial Y} = 0 \tag{15}$$

$$\frac{1}{\varepsilon^2}\left[U\frac{\partial U}{\partial X} + V\frac{\partial U}{\partial Y}\right] = -\frac{\partial P}{\partial X} + \frac{\rho_f}{\rho_{nf}}\frac{\mu_{nf}}{\mu}\frac{R_\mu}{Re}\left(\frac{\partial^2 U}{\partial X^2} + \frac{\partial^2 U}{\partial Y^2}\right) - \frac{\rho_f}{\rho_{nf}}\frac{\mu_{nf}}{\mu}\frac{1}{Re\,Da}U - \frac{C}{\sqrt{Da}}\left|\vec{V}\right|U + Ri\theta + \frac{\rho_f}{\rho_{nf}}Mn(\Upsilon_c - \theta - \Upsilon_i)\bar{H}\frac{\partial \bar{H}}{\partial X} \tag{16a}$$

$$\frac{1}{\varepsilon^2}\left[U\frac{\partial V}{\partial X} + V\frac{\partial V}{\partial Y}\right] = -\frac{\partial P}{\partial Y} + \frac{\rho_f}{\rho_{nf}}\frac{\mu_{nf}}{\mu}\frac{R_\mu}{Re}\left(\frac{\partial^2 V}{\partial X^2} + \frac{\partial^2 V}{\partial Y^2}\right) - \frac{\rho_f}{\rho_{nf}}\frac{\mu_{nf}}{\mu}\frac{1}{Re\,Da}V - \frac{C}{\sqrt{Da}}\left|\vec{V}\right|V + \frac{\rho_f}{\rho_{nf}}Mn(\Upsilon_c - \theta - \Upsilon_i)\bar{H}\frac{\partial \bar{H}}{\partial Y} \tag{16b}$$

$$U\frac{\partial \theta}{\partial X} + V\frac{\partial \theta}{\partial Y} = \frac{(\rho C_p)_f}{(\rho C_p)_{nf}}\frac{1}{RePr}\left[\frac{\partial}{\partial X}\left(R_k\frac{k_{nf}}{k_f}\frac{\partial \theta}{\partial X}\right) + \frac{\partial}{\partial Y}\left(R_k\frac{k_{nf}}{k_f}\frac{\partial \theta}{\partial Y}\right)\right] + \frac{(\rho C_p)_f}{(\rho C_p)_{nf}}Mn\,Ec(\Upsilon_c + \theta)\bar{H}\left(U\frac{\partial \bar{H}}{\partial X} + V\frac{\partial \bar{H}}{\partial Y}\right) \tag{17}$$

Inlet: $U = 1, V = 0, \theta = 0$ (18)

Exit: $\frac{\partial U}{\partial X} = 0, V = 0, \frac{\partial \theta}{\partial X} = 0$ (19)

Right wall:
$$U = V = 0 \quad \begin{cases} \frac{\partial \theta}{\partial Y} = -\frac{1}{R_k}\frac{k_f}{k_{nf}} & \text{under the blocks} \\ \frac{\partial \theta}{\partial Y} = 0 & \text{elsewhere} \end{cases} \tag{20}$$

Left wall: $U = V = 0, \frac{\partial \theta}{\partial Y} = 0$ (21)

The expressions of the various dimensionless groupings are as follows:

$$Re = \frac{\rho_f U_i W}{\mu}, Da = \frac{K}{W^2}, Ri = \frac{g\beta\, {}^{qW}/_{k_f}\, W}{U_i^2}$$
$$R_\mu = \frac{\mu_{eff}}{\mu_{nf}}, Mn = \frac{\mu_0 K' H_0^2\, {}^{qW}/_{k_f}}{\rho_f U_i^2}, Pr = \frac{\mu C_p}{k_f}$$
$$Ec = \frac{U_i^2}{C_{pf}\, {}^{qW}/_{k_f}}, \Upsilon_{c,i} = \frac{T_{c,i}}{{}^{qW}/_{k_f}}, R_k = \frac{k_{eff}}{k_{nf}}$$

2.6 Nusselt Number

The local Nusselt number is calculated as follows:

$$Nu = \frac{1}{\theta_w} \tag{22}$$

The mean Nusselt number at the level of each block is computed as the following:

$$Nu_{mi} = \frac{1}{W_p}\int_{X_i}^{X_i+W_p} Nu\, dX \tag{23}$$

Where X_i is the position of block "i" relative to the channel inlet.

The global Nusselt number is determined as follows:

$$Nu_g = \frac{1}{3}\sum_{i=1}^{i=3} Nu_{mi} \tag{24}$$

2.7 Friction Coefficient

The local friction coefficient is given by:

$$f = -\frac{\rho_{nf}}{\rho_f}\frac{dP_m}{dX}\frac{1}{U_m^2}$$
$$P_m = \int_0^1 P\, dY, U_m = \int_0^1 U\, dY \tag{25}$$

The mean friction coefficient is expressed as:

$$f_m = \frac{1}{L}\int_0^L f\, dX \tag{26}$$

2.8 Performance Factor

The efficiency of the different heat transfer enhancement techniques used in this study is analyzed by introducing a global Nusselt number ratio η_{Nug} and a mean friction coefficient ratio η_{fm}. For this purpose, Nu_g and f_m are normalized by their respective values obtained for a reference case corresponding to a classical mixed convection problem (Ri = 1) of a (water-Fe_3O_4) ferrofluid in a vertical channel without a magnetic field (Mn = 0) and with rectangular-shaped porous blocks ($Da=10^{-2}$ and H_p = 0.6). These two ratios are calculated as follows:

$$\eta_{Nug} = \frac{Nu_g}{Nu_{gref}} \tag{27}$$

$$\eta_{fm} = \frac{f_m}{f_{mref}} \tag{28}$$

Gains and losses in heat transfer and pressure drop are compared by introducing the performance factor, defined as follows:

$$R_\eta = \frac{\eta_{Nug}}{\eta_{fm}} \tag{29}$$

3. NUMERICAL PROCEDURE

The governing Eqs. (15) - (17) with their boundary conditions (18) - (21) are numerically solved by the finite volume method (Patankar 1980). A staggered mesh is employed such that the components of velocity are situated on the control volume interfaces while the pressure and temperature are located in the control volume centers. Velocity and pressure fields are coupled by the SIMPLE algorithm, and the power-law scheme is utilized in the discretization process. The obtained system of algebraic equations is then solved by the line-by-line technique, which combines the Gauss-Seidel method and the tridiagonal matrix algorithm. A non-uniform mesh, in the axial and transverse directions, is employed with the most refined meshes near the solid walls and in the interfacial regions of the porous blocks. Different mesh systems were tested to examine the impact of the grid size on the numerical solution, and a typical case is shown in Table 3. From a 480×70 mesh (in the X and Y directions, respectively), the solution becomes slightly sensitive to the increase of nodes number since the relative variations on the global Nusselt numbers and the mean friction coefficients do not exceed 1%. For the iterative process stop, the chosen convergence criterion is the maximum relative error between two successive iterations for the velocity components and temperature, which must be less than 10^{-5}.

Table 3 Grid sensitivity analysis for the triangular shape: Da = 10^{-2}, Ri = 1 and Mn =30

	240×50	320×50	400×60	480×60	480×70	480×80
Nu_g	34.16	31.13	30.01	29.04	28.69	28.47
Relative error (%)	-	8.87	3.60	3.23	1.20	0.77
f_m	0.053	0.101	0.157	0.169	0.168	0.167
Relative error (%)	-	90.57	55.44	7.64	0.59	0.59

The reliability of the developed computational code was verified by comparing our results with those obtained by Ganguly *et al*. (2004). They conducted a numerical investigation of ferrofluid forced convection under a variable magnetic field. The second comparison is made with Behnampour *et al.* (2017), who numerically studied the convective heat exchange of (water-Ag) nanofluid inside a channel with solid blocks of different shapes. The third validation is done with the results of Jarray *et al.* (2020) in a porous medium under the effect of a magnetic source. Figures 2 and 3 and Table 4 show good agreements between the different results.

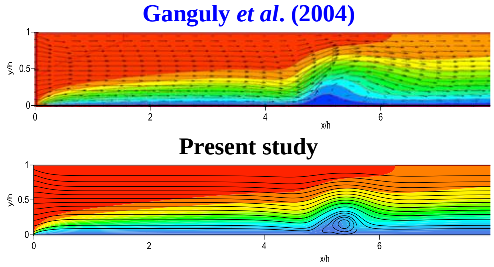

Fig. 2. Streamlines and isotherms for Re = 12 and Ri = 0.

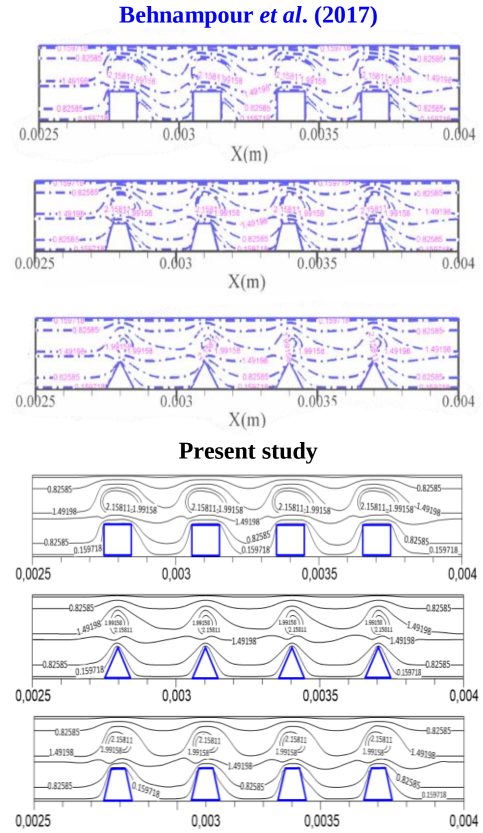

Fig. 3. Dimensionless axial velocity lines for different block shapes: H_p = 0.4, Re = 50, Ri = 0, Mn = 0 and φ = 0.04.

Table 4 Mean Nusselt number for Re = 500, Da = 10^{-2}, φ = 0.05, Gr = 10^4, Ec = 10^{-3} and Pr = 6.2

Mn	0	20	40	60	80	100
Present study	8.08	8.09	8.12	8.22	8.30	8.37
Jarray *et al.* (2020)	8.09	8.14	8.23	8.29	8.35	8.40
Relative error (%)	0.12	0.61	1.34	0.84	0.60	0.36

4. RESULTS

Since the governing parameters of the problem under investigation are numerous, some of them have been fixed: the base fluid is water Pr = 6.62, the porosity ε = 0.97, the inertial coefficient C = 0.1, the Reynolds number Re = 200, the Darcy number Da = 10^{-2}, the viscosity ratio $R_\mu = 1$, and the thermal conductivity ratio $R_k = 1$. The geometrical parameters are as follows: the length of the channel is L = 29, the base width of a porous block is $W_p = 1$, and the spacing between two successive blocks is $S_p = 1$. Furthermore, we focused on the effect of the magnetic number ($0 \leq Mn \leq 50$), the porous blocks shape (rectangular, trapezoidal, and triangular), and the Richardson number ($1 \leq Ri \leq 50$). The presented results are mainly for the variable volume (VV) case, and only the last section is devoted to the comparison between the variable volume (VV) and the constant volume (CV) cases.

The impact of the magnetic number, reflecting the ferrohydrodynamics effect, on the streamlines and isotherms for different block shapes is illustrated in Fig. 4. With no magnetic field and considering the porous medium permeability, the flow occurs in the blocks with slight resistance and freely outside. The ferrofluid motion is disrupted when the sources are activated, and this disturbance is slight and localized around the plate containing the porous blocks at low Mn values before amplifying and expanding throughout the entire height of the channel in the blocks' region. At large values of the magnetic number, recirculation zones appear in the vicinity of the sources regardless of the blocks' shape. This flow structure, at high Mn, is favorable to the ferrofluid mixing, as shown in the isotherms, which has a beneficial effect on thermal exchanges. The appearance of these rotating fluid masses can be explained in the following way: under the magnetic field's effect, Fe_3O_4 nanoparticles become magnetized, and the fluid is then attracted towards the heat sources. The nanoparticles' magnetization decreases by approaching the latter, and there is a migration to the less hot regions where the magnetization effect is once more amplified. This oscillation between increased and decreased magnetization is the root cause of these recirculation zones' formation, which allows the transport of the calorific energy released by the heat sources. This figure shows that the dynamic and thermal fields are also affected by the shape of the porous blocks. Indeed, for low Mn values, the magnetic field effect is weak, and the porous medium contributes most to the heat transfer between the ferrofluid and the hot sources. In this case, the best cooling is obtained with rectangular blocks because of their large exchange surface, double that of the triangular shape. For Mn > 5, the magnetic field – blocks shape interaction is more important for the triangular blocks, which leads to higher cooling efficiency. At large Mn, the magnetic field overcame the resistance created by the porous medium regardless of the shape type; however, better fluid mixing occurs when the blocks are shaped triangularly.

The local Nusselt number evolution along the channel for different Mn and various block shapes is shown in Fig. 5. The heat transfer is maximal at each block leading edge and then decreases due to the development of boundary layers. This evolution is interrupted when approaching the magnetic sources due to the disturbances caused to the flow by the latter; the transfer is then improved, and the Nusselt number increases. The rise of the magnetic number accentuates this effect, and the local values of Nu exceed those obtained at the leading edge of each block for the triangular shape, exhibiting the lowest flow resistance caused by the porous medium.

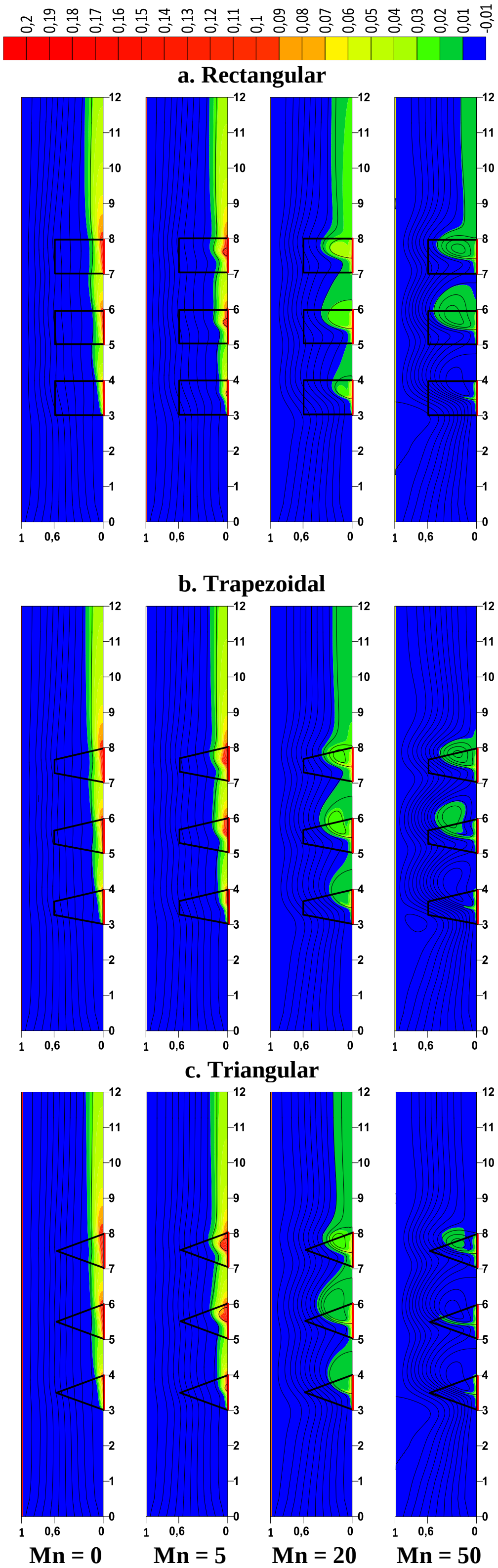

Fig. 4. Streamlines and isotherms for for various Mn values and block shapes: Ri = 1.

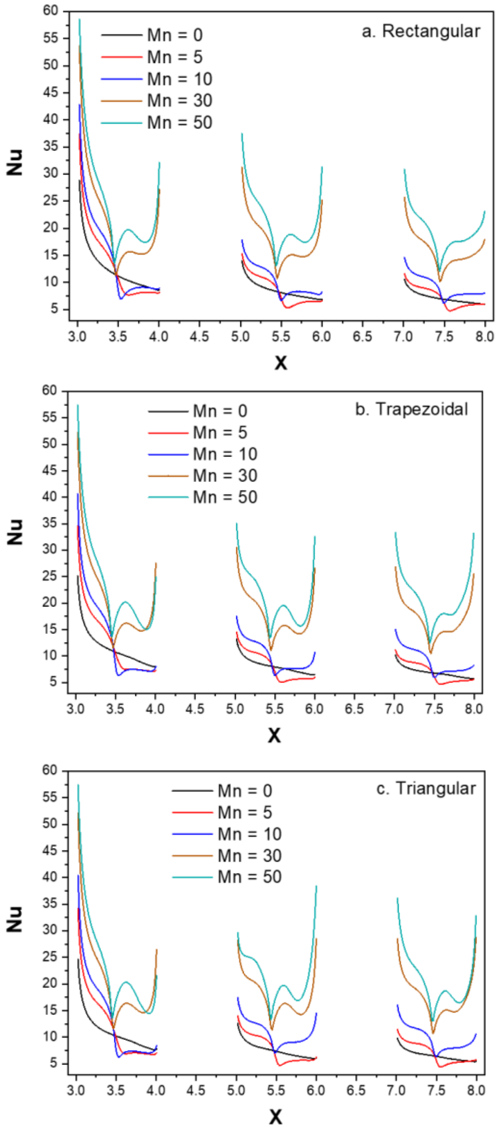

Fig. 5. Local Nusselt number for various Mn and block shapes: Ri = 1.

The variation of the global Nusselt number with Mn for various block shapes is depicted in Fig. 6a. It can be seen that an augmentation in the magnetic field strength is advantageous to the heat transfer regardless of the form. Indeed, the sources' activation causes the migration of Fe_3O_4 nanoparticles towards the heated regions due to their magnetization, leading to a higher local thermal conductivity and, consequently, increased local heat transfer. The other aspect emerging from this figure is that although the influence of the porous blocks' shape is much less apparent than that of the magnetic field, it changes with varying magnetic number values. Thus, the rectangular shape is thermally the most efficient at low Mn. Due to the high Darcy number, the fluid penetrates the blocks in significant amounts, resulting in a large exchange surface. Hence, the interest of the rectangular blocks' volume, which is twice that of the triangular shape. For Mn > 10, the perturbations created by the sources are more significant, and the triangular shape seems to be, thermally, the most performant since the magnetic field overcomes the resistance induced by the porous medium. At high Mn values, the blocks' shape effect becomes negligible compared to the magnetic field, resulting in very close Nu_g values. The maximum improvement in the heat exchange rate in comparison to the case without a magnetic field is around 132% for the rectangular shape, 146% for the trapezoidal shape, and 160% for the triangular shape. The highest contribution of the blocks' shape to Nu_g increase is achieved at Mn = 20, where the deviation from the rectangular shape is around 3% with a trapezoidal shape and 6% with a triangular shape.

The heat transfer enhancement observed in Fig. 6a is accompanied by an increase in the mean friction coefficient, as shown in Fig. 6b. Indeed, the magnetic field intensity increase is synonymous with the growth of the flow disturbance and thus more pressure losses. The highest f_m values are obtained with the rectangular porous blocks, which present a more significant flow resistance than the other two shapes, especially the triangular blocks, for which the volume is half that of the rectangular blocks. Compared to the case with no magnetic field, the maximum rate of increase is about 45% for the three shapes of porous blocks. f_m reduces by 17% and 30% with the trapezoidal and triangular blocks, respectively, compared to the rectangular shape.

The current outcomes on the impact of a variable magnetic field and its intensity on the flow and heat transfer characteristics are qualitatively comparable to those of several earlier research works (Ganguly *et al.* 2004; Ghasemian *et al.* 2015; Nessab *et al.* 2019; Jarray *et al.* 2020; Mehrez and El Cafsi 2021; Dahmani *et al.* 2022) despite the difference in the study conditions.

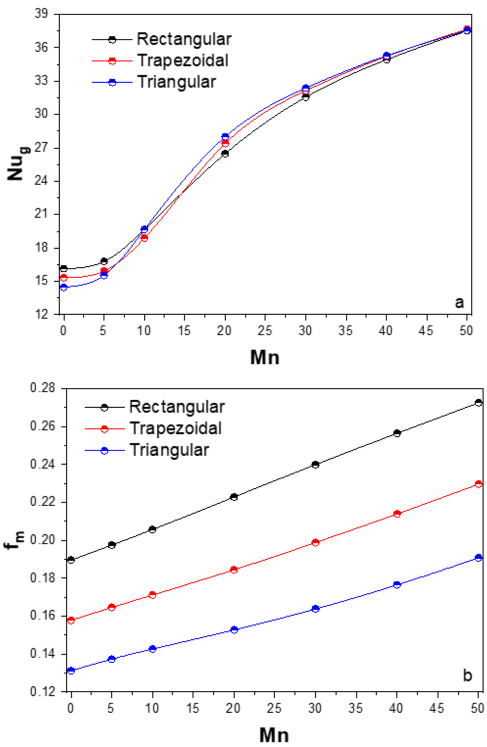

Fig. 6. Evolution of Nu_g and f_m with Mn for different block shapes: Ri = 1.

To highlight the interest in the interaction between the magnetic field and the blocks' shape, we present in Fig. 7 the evolutions of the global Nusselt number ratio η_{Nug} and the mean friction coefficient ratio η_{fm}. According to Fig. 7a, for Mn < 5, the reference case is thermally interesting for trapezoidal or triangular-shaped blocks and slightly less efficient for the rectangular shape. Beyond this magnetic number range, the dual technique seems beneficial regardless of the magnetic field strength and the form of the porous blocks. A maximum improvement of 133% is reached at Mn = 50, and the shape effect is most noticeable at Mn = 20. Figure 7b shows the impact of these techniques' combination on the mean friction coefficient, which is efficient for the trapezoidal shape for Mn values below 25 and for the triangular shape, whatever Mn values.

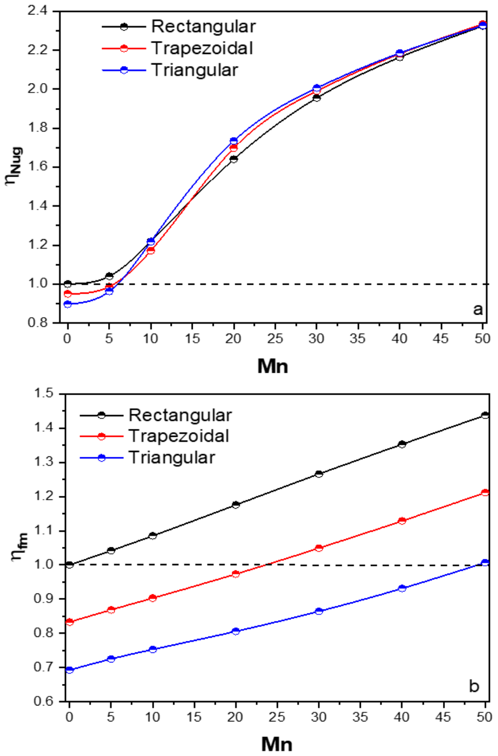

Fig. 7. Evolution of η_{Nug} and η_{fm} with Mn for different block shapes: Ri = 1.

The performance factor R_η compares the gains or losses between the heat transfer rate and the pressure drop. Figure 8 shows that the enhancement techniques implemented in the thermal system are effective since R_η is always greater than unity for all values of the magnetic number and shapes of the porous blocks. The performance factor rises with Mn, but this increase is weak at low and high magnetic field strengths. The maximum values of R_η are about 1.62, 1.93, and 2.35 for the rectangular, trapezoidal, and triangular shapes, respectively. The triangular shape is the most performant since it leads to high heat transfer rates and low mean friction coefficients.

The second parameter considered is the buoyancy force intensity expressed by the Richardson number. The dynamic and thermal fields' structures for

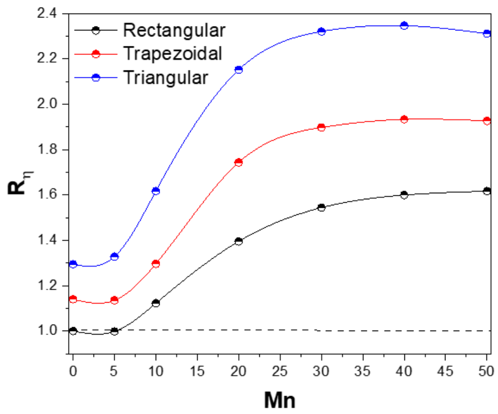

Fig. 8. Evolution of R_η with Mn for different block shapes: Ri = 1.

different Ri and blocks' shapes are initially depicted in Fig. 9. The flow disruption and the recirculation zones resulting from the magnetic field tend to disappear as the Ri value rises, regardless of the porous blocks' shape. Similar behavior has been reported previously by Job and Gunakala (2018) when applying an alternating magnetic field in the presence of porous blocks. Indeed, the buoyancy force, acting on the main flow direction, accelerates the ferrofluid motion, particularly in the heat sources region, and initially suppresses the flow structure induced in the channel by the ferrohydrodynamics effect. As a result, the heat sources' cooling is reduced, and the thickness of the thermal boundary layer increases. By further growing Ri, substantial velocity and temperature gradients are created at the right wall, causing a reduction of the boundary layer thickness and improving the heat sources' cooling again, but less important than that observed at low Richardson numbers. The analysis of the buoyancy force effect associated with the blocks' form exhibits two behaviors. At low Ri, since the triangular shape presents the lowest opposition to the dominant impact of the magnetic field, it is thermally the most efficient. On the other hand, at large values of the Richardson number, the buoyancy force prevails, and the rectangular shape becomes the most performing because of its larger exchange surface.

Figure 10a depicts the global Nusselt number variation with Ri for various block shapes. The heat transfer decreases until it reaches a minimum value around Ri = 7, after which it increases. The explanation of this evolution is as follows: in ferrohydrodynamics mixed convection, there is a competition between the Kelvin force and the buoyancy force. Indeed, the former causes the FHD effect and generates a flow structure beneficial to heat transfer (Fig. 4), while the latter accelerates the ferrofluid motion close to the heat sources (Fig. 9). The magnetic field effect dominates when the Richardson number is low, and in this case, the global Nusselt number is maximal. As buoyancy force increases, the magnetic field effect diminishes until it vanishes, decreasing thereby heat transfer rate. Beyond the critical Ri value, the buoyancy force takes over, the fluid flow near the wall containing the porous blocks is accelerated, and the heat transfer is improved, but not to the same level as at low Ri.

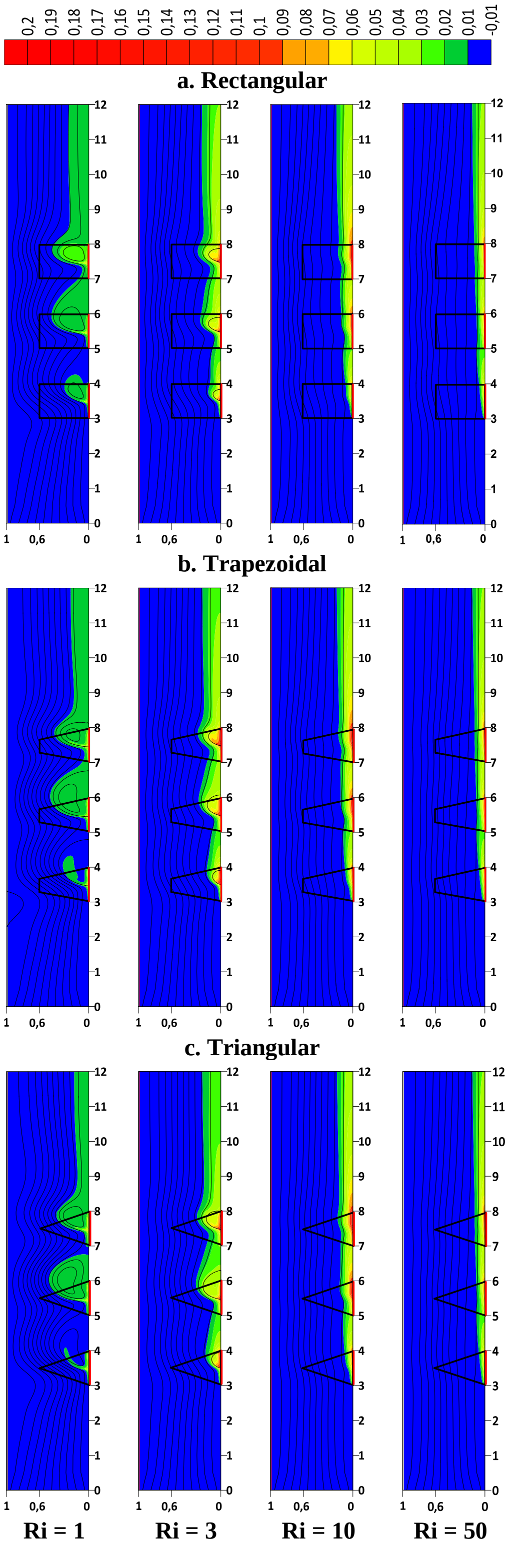

Fig. 9. Streamlines and isotherms for various Ri values and block shapes: Mn = 30.

Although the effect of the porous blocks' shape is less noticeable than that of Ri, the triangular shape appears to be the most efficient for Richardson numbers less than 3, owing to its low resistance to the magnetic field action. Beyond this value, the trend reverses, and the rectangular shape, with the larger exchange surface, becomes the optimal shape.

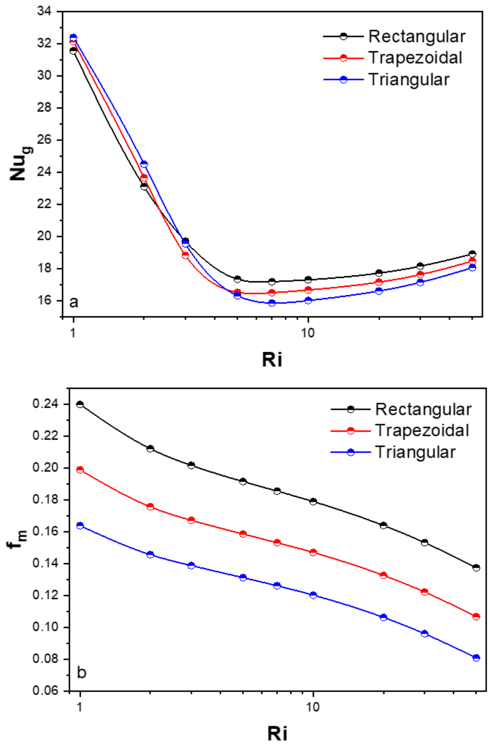

Fig. 10. Evolution of Nu_g and f_m with Ri for different block shapes: Mn = 30.

The increase of Ri reduces the resistance to the flow and decreases the mean friction coefficient, as shown in Fig. 10b. This behavior is found whatever the shape, with the highest values of f_m for the rectangular blocks and the lowest ones for the triangular shape, the reason being the reduction in volume.

As seen in Fig. 11, the critical Richardson number beyond which the buoyancy force exceeds the Kelvin force rises with increasing magnetic number. Indeed, to overcome the substantial effect of the magnetic field at high Mn, a progressively higher Ri will be required. The value of this critical Richardson number is about 3, 5, 7, and 10 for Mn = 5, 15, 30, and 50, respectively. The global Nusselt number becomes insensitive to changes in the Kelvin force at large values of buoyancy force; as a result, the curves merge.

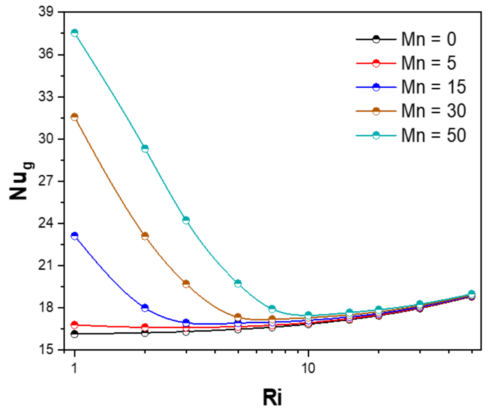

Fig. 11. Evolution of Nu_g with Ri for the rectangular shape and different values of Mn.

Figure 12a shows that the combined effect of the magnetic field, the buoyancy force, and the shape of the blocks are beneficial to the heat exchange since the Nu_g ratio is overall greater than unity regardless of the considered situation. The maximum improvement compared to the reference case, about 101%, is obtained with the triangular shape at Ri = 1. When the buoyancy force dominates over the action of the magnetic field, the rectangular shape produces the most significant ratio, which is roughly 1.17 at Ri = 50.

The mean friction coefficient ratio, shown in Fig. 12b, highlights the benefit of the triangular shape regardless of the Ri value and the advantage of the other forms beyond Ri ≈ 1.5 for the trapezoidal blocks and Ri ≈ 5 for the rectangular blocks. For the triangular blocks, the gain in pressure drop increases from 14% to 57% by varying the Richardson number from 1 to 50. The maximum profits, obtained at Ri = 50, are roughly 44% and 28% for the trapezoidal and rectangular shapes, respectively.

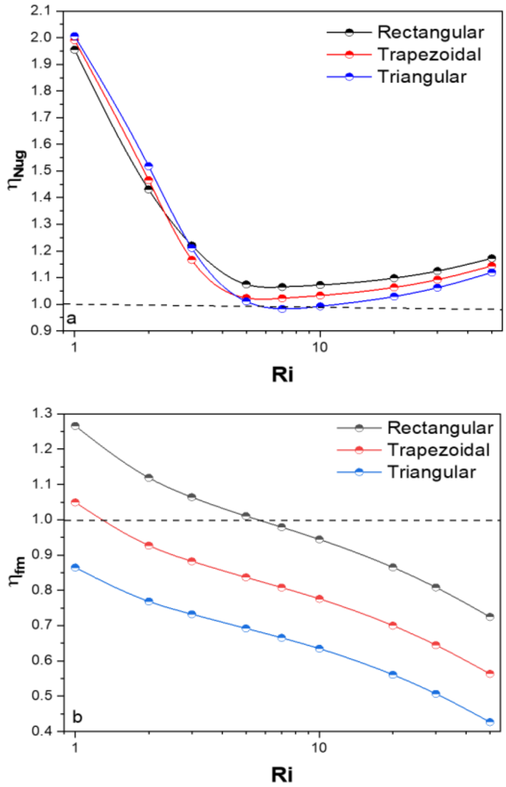

Fig. 12. Variation of η_{Nug} and η_{fm} with Ri for various block shapes: Mn = 30.

Figure 13 reveals that regardless of the Ri value or the blocks' shape, the performance factor is more than unity; this is a direct consequence of the results shown in Fig. 12, which indicate a simultaneous gain in heat transfer and pressure drop. R_η declines in value at first, reaching a minimum around Ri = 5, then increasing and surpassing the value at Ri = 1. At dominant magnetic field, the performance factor values are 2.32, 1.90, and 1.54 for triangular, trapezoidal, and rectangular shapes, respectively. At dominant buoyancy force, the values of R_η increase to 2.62, 2.03, and 1.62.

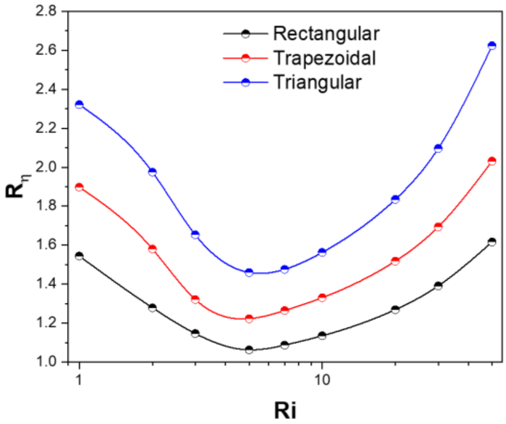

Fig. 13. Evolution of R_η with Ri for different block shapes: Mn = 30.

Till now, we have considered that the passage from one shape to another was accomplished by keeping the blocks' height constant while reducing the volume. The form can be altered by maintaining the volume constant and adjusting the height. The following figures compare the two methods, taking the volume of the triangular shape with H_p = 0.6 as a reference.

Figure 14 shows the evolution of the Nu_g and f_m ratios with Mn for the rectangular and trapezoidal shapes. Analyzing these ratios can assess the impact of the porous blocks' height. The magnetic field influence is not very important at low Mn values, so heat transfer is controlled by the exchange surface of the porous blocks, which is more significant in the VV case, resulting in Nu_g ratios greater than unity. The impact of block height is reduced as the magnetic field intensity increases, and at roughly Mn = 10, this ratio is slightly less than 1, indicating that the CV case with a lower block height contributes more to heat transfer. Beyond the values of Mn = 12.5 for trapezoidal blocks and Mn = 20 for rectangular blocks, the impact of the magnetic field dominates that of the blocks' height, thus suppressing the effect of the porous medium. Consequently, the heat transfer rates for the VV and CV cases tend to be identical.

The examination of Fig. 14b reveals a mean friction coefficient ratio greater than unity regardless of the magnetic number value. This behavior is because of the greater block height in the case of the variable volume. This ratio also increases with Mn due to the perturbations created by the magnetic field. Comparison between the two block shapes shows lower rates with the trapezoidal blocks due to the block heights for the VV and CV cases being closer in this situation (see Table 1).

Figure 15 depicts the evolution of the two ratios with the Richardson number. At low Ri, as previously found, the effect of the magnetic field is significant, and the porous medium's contribution to heat transfer is neglected. There is, however, a better heat exchange for the blocks at a low height corresponding to the CV case. From a Ri number, between 2 and 3, depending on the blocks' shape, the Nu_g ratio increases and exceeds unity at Ri ≈ 2.5 for

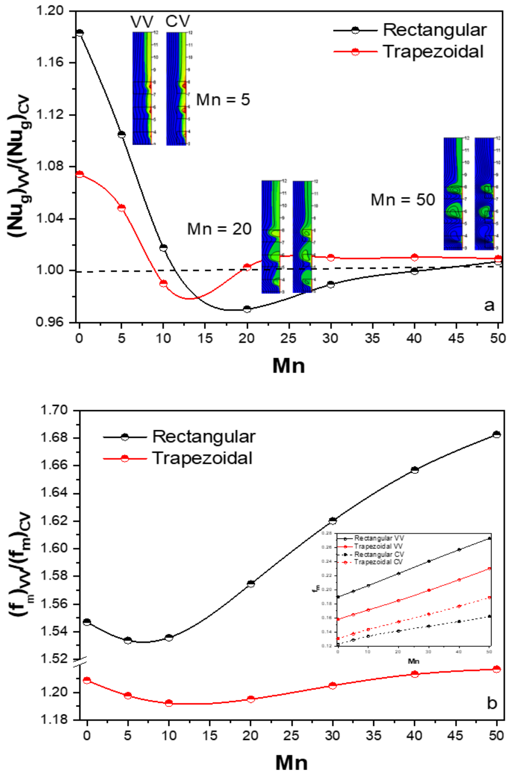

Fig. 14. Evolution of $(Nu_g)_{VV}/(Nu_g)_{CV}$ and $(f_m)_{VV}/(f_m)_{CV}$ with Mn for different block shapes: Ri = 1.

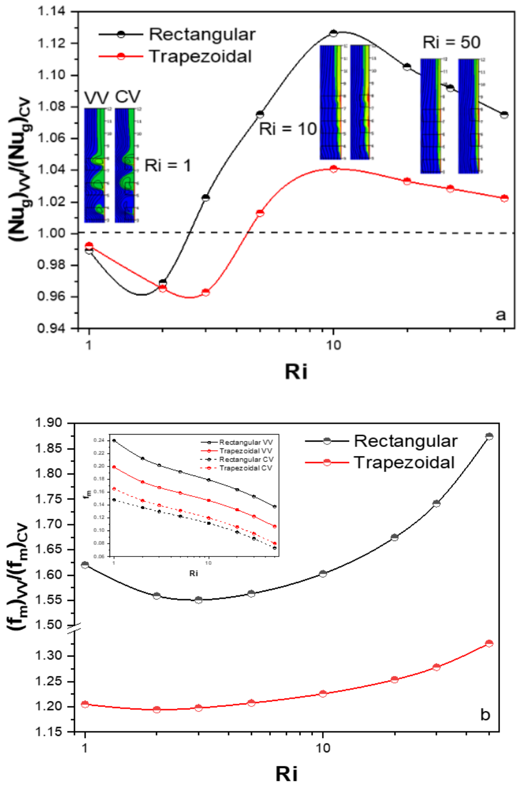

Fig. 15. Evolution of $(Nu_g)_{VV}/(Nu_g)_{CV}$ and $(f_m)_{VV}/(f_m)_{CV}$ with Ri for different block shapes: Mn = 30.

rectangular blocks and Ri ≈ 4.5 for trapezoidal blocks. Indeed, rising the buoyancy force causes the nanofluid flow to accelerate near the heat sources, reducing the magnetic field impact and favoring the porous medium, which has a larger exchange surface in the VV case. For Ri > 10, the magnetic field influence is eliminated, and the flow resistance in the porous blocks is reduced, so the Nu_g ratio decreases although it remains higher than unity.

Though the mean friction coefficients decrease with increasing Ri, their ratios grow with this control parameter having values greater than unity. This behavior is attributed to the big impact of the blocks' volume on f_m, even though the flow is accelerated at large Ri.

5. Conclusions

FHD mixed convection flow of (Fe_3O_4-water) ferrofluid inside a vertical channel containing variously shaped heated porous blocks has been numerically investigated. The key findings are as follows:

- Increasing the magnetic number disrupts the ferrofluid flow, but the influence of the magnetic field fades as the Richardson number grows.

- The heat transfer is improved by increasing the magnetic field strength. However, its evolution with the buoyancy force is non-monotonic since it decreases with Ri until it reaches a minimum value that rises with Mn before increasing again.

- Thermally, rectangular blocks are the most efficient at low Mn and high Ri. In contrast, the triangular shape is the most beneficial at moderate and small magnetic and Richardson numbers values, respectively. When the intensity of the magnetic field is high, the impact of the blocks' shape disappears.

- The mean friction coefficient, whose values are the most important for the rectangular blocks, increases with increased Mn and reduced Ri.

- By activating the magnetic sources, the maximum enhancement in heat transfer rate is around 132% for the rectangular blocks, 146% for the trapezoidal blocks, and 160% for the triangular blocks. The highest increase in pressure drop is about 45% for all considered shapes.

- Regardless of the Ri and Mn values or the blocks' shape, the performance factor is more than unity, with the triangular shape being the most performant since it leads to high heat transfer rates and low mean friction coefficients. The triangular shape also performed best in previous studies under different conditions (Guerroudj and Kahalerras 2010; Guerroudj and Kahalerras 2012; Seo *et al.* 2014; Behnampour *et al.* 2017; Shamsi *et al.* 2017).

- Thermally, the VV case is the most efficient at low Mn and moderate to high Ri, whereas the CV case globally becomes so for the other magnetic and Richardson numbers values. The effect of the porous medium disappears at high magnetic field strength, resulting in similar heat transfer rates regardless of blocks height.

- Compared to the constant volume case, the variable volume case leads to higher values of the mean friction coefficients, with the f_m ratio increasing as Mn and Ri rise.

The present work might be extended to include the entropy generation analysis, other blocks' shapes, the porous medium's nature, pulsating flow, MHD and FHD coupled effects, and performing an experimental investigation on a real electronic device. For instance, using a (Fe_3O_4-Cu/water) hybrid nanofluid is advised to remedy the problem of the low thermal conductivity of magnetite nanoparticles. These expansions will improve the current study's computational outcomes and broaden their potential applications.

REFERENCES

Ali, F. H., H. K. Hamzah, A. K. Hussein, M. Y. Jabbar and P. Talebizadehsardari (2020). MHD mixed convection due to a rotating circular cylinder in a trapezoidal enclosure filled with a nanofluid saturated with a porous media. *International Journal of Mechanical Sciences* 181,105688.

Alsedais, N., A. M. Aly and M. A. Mansour (2022). Local thermal non-equilibrium condition on mixed convection of a nanofluid-filled undulating cavity containing obstacle and saturated by porous media. *Ain Shams Engineering Journal* 13, 101562.

Alves, L. S. de B., A. Barletta, S. Hirata and M. N. Ouarzazi (2014). Effects of viscous dissipation on the convective instability of viscoelstic mixed convection flows in porous media. *International Journal of Heat and Mass Transfer* 70, 104457.

Aly, A. M. and S. E. Ahmed (2020). ISPH simulations for a variable magneto-convective flow of a ferrofluid in a closed space includes open circular pipes. *International Communications in Heat and Mass Transfer* 110, 104412.

Behnampour, A., O. A. Akbari, M. R. Safaei, M. Ghavami, A. Marzban, G. A. Sheikh Shabani, M. Zarringhalam and R. Mashayekhi (2017). Analysis of heat transfer and nanofluid fluid flow in microchannels with trapezoidal, rectangular and triangular shaped ribs. *Physica E: Low-dimensional Systems and Nanostructures* 91, 15-31.

Bondarenko, D. S., M. A. Sheremet, H. F. Oztop and N. Abu-Hamdeh (2019). Mixed convection heat transfer of a nanofluid in a lid-driven enclosure with two adherent porous blocks. *Journal of Thermal Analysis and Calorimetry* 135, 1095-1105.

Chakkingal, M., J. de Geus, S. Kenjereš. I. Ataei-Dadavi, M. J. Tummers and C. R. Kleijn (2020). Assisting and opposing mixed convection with conjugate heat transfer in a differentially heated cavity filled with coarse-grained porous media. *International Communications in Heat and Mass Transfer* 111, 586-598.

Çolak, E., Ö. Ekici and H. F. Öztop (2021). Mixed convection in a lid-driven cavity with partially heated porous block. *International Communications in Heat and Mass Transfer* 126, 105450.

Corcione, M. (2011). Empirical correlating equations for predicting the effective thermal conductivity and dynamic viscosity of nanofluids. *Energy Conversion and Management* 52(1), 789-793.

Dahmani, A., J. Muñoz-Càmara, S. Laouedj and J. P. Solano (2022). Heat transfer enhancement of ferrofluid flow in a solar absorber tube under a periodic current-carrying wire. *Sustainable Energy Technologies and Assessments* 52, 101996.

Ganguly, R., S. Sen and I. Puri (2004). Heat transfer augmentation using a magnetic fluid under the influence of a line dipole. *Journal of Magnetism and Magnetic Materials* 271(1), 63-73.

Ghalambaz, M., M. Sabour, S. Sazgar, I. Pop and R. Trâmbiţaş (2020). Insight into the dynamics of ferrohydrodynamic (FHD) and magnetohydrodynamic (MHD) nanofluids inside a hexagonal cavity in the presence of a non-uniform magnetic field. *Journal of Magnetism and Magnetic Materials* 497, 166024.

Ghasemian, M., Z. Najafian Ashrafi, M. Goharkhah and M. Ashjaee (2015). Heat transfer characteristics of Fe_3O_4 ferrofluid flowing in a mini channel under constant and alternating magnetic fields. *Journal of Magnetism and Magnetic Materials* 381, 158-167.

Ghorbani, B., S. Ebrahimi and K. Vijayaraghavan (2018). CFD modeling and sensitivity analysis of heat transfer enhancement of a ferrofluid flow in the presence of a magnetic field. *International Journal of Heat and Mass Transfer* 127, 544-552.

Gibanov, N. S., M. A. Sheremet, H. F. Oztop and O. K. Nusier (2017). Convective heat transfer of ferrofluid in a lid-driven cavity with a heat-conducting solid backward step under the effect of a variable magnetic field. *Numerical Heat Transfer, Part A: Applications* 72(1), 54-67.

Guerroudj, N. and H. Kahalerras (2010). Mixed convection in a channel provided with porous blocks of various shapes. *Energy Conversion and Management* 51(3), 505-517.

Guerroudj, N. and H. Kahalerras (2012). Mixed convection in an inclined channel with heated porous blocks. *International Journal of Numerical Methods for Heat and Fluid Flow* 22, 839-861.

Jakeer, S., P. B. A. Reddy, A. M. Rashad and H. A. Nabwey (2021). Impact of heated obstacle position on magneto-hybrid nanofluid flow in a lid-driven porous cavity with Cattaneo-Christov heat flux pattern. *Alexandria Engineering Journal* 60, 821-835.

Jarray, A., Z. Mehrez and A. El Cafsi (2020). Effect of magnetic field on the mixed convection Fe_3O_4/water ferrofluid flow in a horizontal porous channel. *Pramana – Journal of Physics* 94, 156-167.

Job, V. M. and S. R. Gunakala (2018). Mixed convective ferrofluid flow through a corrugated channel with wall-mounted porous blocks under an alternating magnetic field. *International Journal of Mechanical Sciences* 144, 357-381.

Khetib, Y., K. Sedraoui, A. A. Melaibari, A. Elzaied, R. Alsulami and M. Sharifpur (2021). Heat transfer and pressure drop in turbulent nanofluid flow in a pin-fin heat sink: Fin and nanoparticles shape effects. *Case Studies in Thermal Engineering* 28, 101378.

Larimi, M. M., A. Ghanaat, A. Ramiar and A. A. Ranjbar (2016). Forced convection heat transfer in a channel under the influence of various non-uniform transverse magnetic field arrangements. *International Journal of Mechanical Sciences* 118, 101-112.

Liu, X., Y. A. Rothan, S. Althobalti and M. M. Selim (2022). Simulation based on FEM for iron oxide–water nanomaterial transportation with involve of a wire as magnetic source. *Applied Nanoscience* https://doi.org/10.1007/s13204-022-02362-4.

Mehrez, Z. and A. El Cafsi (2021). Heat exchange enhancement of ferrofluid flow into rectangular channel in the presence of a magnetic field. *Applied Mathematics and Computation* 391, 125634.

Mejni, F. and M. N. Ouarzazi (2009). Global instabilities in inhomogeneous mixed convection flows in semi-infinite porous media. *Mechanics Research Communications* 36, 260-264.

Mousavi, S. M., M. Biglarian, A. A. R. Darzi, M. Farhadi, H. H. Afrouzi and D. Toghraie (2020). Heat transfer enhancement of ferrofluid flow within a wavy channel by applying a non-uniform magnetic field. *Journal of Thermal Analysis and Calorimetry* 139, 3331-3343.

Nessab, W., H. Kahalerras, B. Fersadou and D. Hammoudi (2019). Numerical investigation of ferrofluid jet flow and convective heat transfer under the influence of magnetic sources. *Applied Thermal Engineering* 150, 271-284.

Nield, D. A. and A. Bejan (2013). *Convection in porous media*. Springer, New York.

Pal, D. and B. Talukdar (2011). Combined effects of Joule heating and chemical reaction on unsteady magnetohydrodynamic mixed convection of a viscous dissipating fluid over a vertical plate in porous media with thermal radiation. *Mathematical and Computer Modelling* 54 (11-12), 3016-3036.

Patankar, S. V. (1980). *Numerical heat transfer and fluid flow*. Mc Graw-Hill, New York.

Pishkar, I., B. Ghasemi, A. Raisi and S. M. Aminossadati (2022). Simulation of variable magnetic field effect on natural convection heat transfer of Fe_3O_4/graphite slurry based on experimental properties of slurries. *Journal of Applied Fluid Mechanics* 15(1), 1-14.

Rosenweig, R. E. (2013). *Ferrohydrodynamics*. Dover Publications, New York.

Seo, H. S., J. C. Lee, I. J. Hwang and Y. J. Kim (2014). Flow characteristics of ferrofluid in a microchannel with patterned blocks. *Materials Research Bulletin* 58, 10-14.

Shah, R. K. and S. Khandekar (2019). Exploring ferrofluids for heat transfer augmentation. *Journal of Magnetism and Magnetic Materials* 475, 389-400.

Shaker, H., M. Abbasalizadeha, S. Khalilarya and S. Y. Motlagh (2021). Two-phase modeling of the effect of non-uniform magnetic field on mixed convection of magnetic nanofluid inside an open cavity. *International Journal of Mechanical Sciences* 207, 106666.

Shamsi, M. R., O. A. Akbari, A. Marzban, D. Toghraie and R. Mashayekhi (2017). Increasing heat transfer of non-Newtonian nanofluid in rectangular microchannel with triangular ribs. *Physica E: Low-Dimensional Systems and Nanostructures* 93, 167-178.

Sheikholeslami, M. and D. D. Ganji (2014). Ferrohydrodynamic and magnetohydrodynamic effects on ferrofluid flow and convective heat transfer. *Energy* 75, 400-410.

Sheikholeslami, M. and S. A. Shehzad (2018). Numerical analysis of Fe_3O_4–H_2O nanofluid flow in permeable media under the effect of external magnetic source. *International Journal of Heat and Mass Transfer* 118, 182-192.

Sheikholeslami, M., D. D. Ganji and M. M. Rashidi (2015). Ferrofluid flow and heat transfer in a semi annulus enclosure in the presence of magnetic source considering thermal radiation. *Journal of the Taiwan Institute of Chemical Engineers* 47, 6-17.

Soltanipour, H. (2021). Numerical analysis of two-phase ferrofluid forced convection in an annulus subjected to magnetic sources. *Applied Thermal Engineering* 196, 117278.

Teimouri, K., M. R. Tavakoli, A. Ghafari and K. C. Kim (2021). Investigation of the plaque morphology effect on changes of pulsatile blood flow in a stenosed curved artery induced by an external magnetic field. *Computers in Biology and Medicine* 135, 104600.

Teimouri, K., M. R. Tavakoli, A. Ghafari and K. C. Kim (2022). Effect of plaque geometry on targeted delivery of stem cells containing magnetic particles in a rigid and elastic curved artery with stenosis. *Journal of Magnetism and Magnetic Materials* 542, 168580.

Tiwari, R. K. and M. K. Das (2007). Heat transfer augmentation in a two-sided lid-driven differentially heated square cavity utilizing nanofluids. *International Journal of Heat and Mass Transfer* 50 (9-10), 2002-2018.

Tzirtzilakis, E. E. (2005). A mathematical model for blood flow in magnetic field. *Physics of Fluids* 17, 077103.

Vafai, K. and C. L. Tien (1981). Boundary and inertia effects on flow and heat transfer in porous media. *International Journal of Heat and Mass Transfer* 24, 193-203.

Vijay, N. and K. Sharma (2022). Heat and mass transfer study of ferrofluid flow between co-rotating stretchable disks with geothermal viscosity: HAM analysis. *Chinese Journal of Physics* 78, 83-95.

Yerramalle, V., B. Premachandran and P. Talukdar (2021). Mixed convection from a heat source in a channel with a porous insert: A numerical analysis based on local thermal non-equilibrium model. *Thermal Science and Engineering Progress* 25, 101010.